General Disclaimer

One or more of the Following Statements may affect this Document

- This document has been reproduced from the best copy furnished by the organizational source. It is being released in the interest of making available as much information as possible.

- This document may contain data, which exceeds the sheet parameters. It was furnished in this condition by the organizational source and is the best copy available.

- This document may contain tone-on-tone or color graphs, charts and/or pictures, which have been reproduced in black and white.

- This document is paginated as submitted by the original source.

- Portions of this document are not fully legible due to the historical nature of some of the material. However, it is the best reproduction available from the original submission.

SU-SEL-68-044

Protonospheric Electron Concentration Profiles

by

A. V. da Rosa
O. K. Garriott

March 1969

Final Report

Prepared under
National Aeronautics and Space
Administration Contract NASr-136

RADIOSCIENCE LABORATORY

STANFORD ELECTRONICS LABORATORIES

STANFORD UNIVERSITY · STANFORD, CALIFORNIA

SU-SEL-68-044

PROTONOSPHERIC ELECTRON CONCENTRATION PROFILES

by

A. V. da Rosa

O. K. Garriott

March 1969

Final Report

Contract NASr-136

National Aeronautics and Space Administration

ABSTRACT

The local electron concentration has been calculated along portions of the orbit of OGO-I, based on "differential Doppler frequency" and Faraday polarization rotation measurements of harmonic radio beacon transmissions. Since it is not possible to make these calculations with sufficient accuracy for most satellite orbits, an extensive error analysis is included, to establish the sources and magnitudes of the uncertainties in the computations. Order-of-magnitude improvement over satellites in low earth orbit is achieved with the very eccentric orbit of OGO-I and by using a combination of Faraday and differential Doppler techniques.

Values of protonospheric electron concentration have been obtained between altitudes of about 6000 and 15000 km on a number of orbits. The uncertainties in the computed values result principally from scaling errors in the Faraday polarization rotation angle and from horizontal gradients in the ionosphere; they typically total less than $\pm$ 600 electrons/cm^3. A number of concentration profiles are shown and are compared with direct probe measurements, with whistler results and with extrapolated values of electron concentration obtained from Alouette I near 1000 km.

TABLE OF CONTENTS

LIST OF TABLES

LIST OF FIGURES

ACKNOWLEDGEMENTS

The present work was supported by NASA contract NASr-136. The authors are very grateful for the cooperation of our Japanese colleagues Professor T. Obayashi and Professor S. Kato as well as our Greek colleague Professor M. Anastassiades who helped with the gathering of some of the data used in this work. We are also indebted to Mr. S.C. Hall who installed the Stanford, Kyoto and Athens sites and provided technical support for the whole operation.

The original concept of the experiment described in this paper was developed in cooperation with Messrs. R.S. Lawrence and E.R. Shiffmacher who were also responsible for the design of the spacecraft hardware.

I - INTRODUCTION

The transmissions of multiple radio beacons from rockets and satellites have been very useful in the study of the ionosphere. When the Doppler shifts at two (or more) coherently related frequencies are compared, the "differential Doppler frequency" is found to be, in general, a function of both the local concentration of electrons near the vehicle and also the rate of change of total electron content between receiver and transmitter. In the case of a near-vertical rocket trajectory, the predominant contribution comes from the local electron concentration and the vertical concentration profile may then be deduced [Seddon, et al. (1954)]. In satellite applications, the contribution from terms proportional to total electron content are usually much larger than the rest, so that it is this quantity which has been evaluated [Ross (1960), de Mendonça (1962)]. Attempts to measure the vertical electron concentration profiles with earth satellites have usually led to erroneous results, principally because the predominant direction of motion is horizontal for most satellites [Ross, et al. (1968)].

If it is desired that the local electron concentration be determined from differential Doppler measurements of satellite radio transmissions, two improvements can be made to increase the reliability of the results:

a. The satellite can be placed in a highly eccentric orbit, so that it has a large vertical velocity component during portions of the trajectory. By appropriate location of the ground receiving station, the satellite will appear to be moving directly away from the receiver for a substantial time, as is the case for a rocket flight.

b. Independent information can be obtained from Faraday rotation measurements which can be used to correct for temporal variations and horizontal gradients in the ionosphere.

In this paper, values of local electron concentration will be computed along portions of the orbit of OGO-I, making use of both of the advantages noted above. An extensive error analysis is performed, in order to properly assess the accuracy of the results and to estimate the magnitude of the various sources of error.

As explained above, the conditions necessary for the measurement of local electron concentration are slow changes in the azimuth and elevation of the satellite as seen from an observing station on the ground. These slow changes must occur while the satellite is at a relatively low altitude range (say 6,000 to 25,000 km) where the electron concentration is still reasonably high. Obviously, such favorable conditions did not occur often, and the results shown in this paper are restricted to only a few passages recorded at Stanford University, when the geometry was most favorable.

OGO-I was launched on 5 September 1964, with an initial perigee altitude of 280 km and an apogee of nearly 149,000 km. By 28 February 1965, the perigee had risen to more than 3,000 km and was continuing upward at about 5,000 km/year. The period was about 64 hours and the orbital inclination was also increasing at about 18 degrees/year. The initial perigee was located at about 20° S latitude.

OGO-I was equipped with a pair of radio beacons operating at harmonically related frequencies (40,01 and 360,09 MHz), which were modulated by 20 - and 200 - kHz signals. The various spectral components had the output powers shown below.

TABLE 1

Frequency (MHz)		Output Power (mw)
40,01	Carrier	230
	Each 200 - kHz sideband	230
	Each 20 - kHz sideband	55
360,09	Carrier	125
	Each 200 - kHz sideband	20
	Each 20 - kHz sideband	12.5

The 40 - MHz transmitting antenna is a simple dipole (gain: 2 db) and the 360 - MHz antenna is a Yagi (gain: 8 db). It was planned to have an earth-stabilized satellite, but difficulties that appeared immediately after launch caused the satellite to spin at a rate of about 5 rpm. This introduced a number of unexpected complications in the interpretation and analysis of the data. The spin-axis orientation is not known precisely. Values of 42.5 degrees in right ascension and -9 degrees in declination, suggested by independent experiments, were used in interpreting the beacon data, although the results do not require an accurate knowledge of this orientation.

II - DATA REDUCTION

The analysis described in this paper is based on the knowledge of two experimentally determined quantities: the time rate of change of the slant columnar content, dI/dt, and the time rate of change of the Faraday rotation angle, $d\Omega/dt$. This section indicates the manner in which these quantities are derived from the raw data obtained from the OGO-I radio beacon signals.

These raw data consist of three main sets of measurements:

1. The amplitude of the 360 MHz VHF signal, received with a circularly polarized antenna.
2. The beat frequency, f_b, between the 40 MHz HF carrier and 1/9 of the frequency of the 360 MHz VHF carrier.
3. The amplitude of the 40 MHz signal, received with a linearly polarized antenna.

To obtain both dI/dt and $d\Omega/dt$, it is necessary to know the spin rate, f_s, of the satellite. This spin rate can be determined by counting the amplitude fades of the 360 MHz carrier which are caused by the rotation of the non-isotropic radiation pattern of the transmitting dipole aboard the satellite.

Consider a signal of frequency f_T, transmitted from a dipole rotating with a spin frequency f_s. Consider also a circularly polarized receiving antenna at a fixed location with respect to the transmitter and assume that the refractive index of the intervening medium does not change with time. The received signal will have a frequency [da Rosa, 1965a]:

$$f_R = f_T \pm f_s$$

where the choice of sign preceding f_s depends on the relative direction of rotation of the dipole and the direction of polarization of the receiving antenna.

If there is relative motion between receiver and transmitter, one may then write

$$f_R = f_T \pm f_s + f_v + f_I \qquad (1)$$

where f_v is the "vacuum Doppler shift" which would be observed in the absence of any ionosphere and f_I is the "ionospheric Doppler shift" which includes all effects of the refracting medium. Thus f_I will include not only the first order effects of phase path reduction and polarization rotation but also the effects of ray refraction. The vacuum Doppler shift is directly proportional to the wave frequency and, at 360 MHz, it is, therefore, 9 times larger than at 40 MHz.

If f_{T40} is the frequency of the transmitted HF carrier then the received HF and VHF carriers have, respectively, the frequencies:

$$f_{R40} = f_{T40} \pm f_s + f_v + f_I \qquad (2)$$

$$f_{R360} = 9\, f_{T40} \pm f_s + 9\, f_v + \frac{1}{9} f_I \qquad (3)$$

The last term in f_{R360} assumes that f_I is proportional to $(1/f)$ which is not quite correct, owing to higher order correction terms discussed below. However, the error is quite insignificant here; in fact, if the entire term $(1/9\ f_I)$ were omitted, the error in the final result would be about 1.3 %. The receiving equipment compares f_{R40} with $(1/9\ f_{R360})$, producing the beat frequency

$$f_b = f_{R40} - (1/9)\ f_{R360} = \frac{80}{81} f_I + A\, f_s \qquad (4)$$

where constant A can assume one of the four values (8/9, - 8/9, 10/9 or -10/9), depending on the sense of polarization of the receiving antennas. With both f_b and f_s measured, f_I can be calculated from equation (4).

Having determined the ionospheric contribution f_I, we wish to relate this to the electron content. In all cases the phase path length is

$$P = \int_p \mu ds \qquad (5)$$

where μ, the refractive index of the medium, has a non-linear dependence on the electron concentration, n. However, in many applications, a linearized expression of μ in terms of n is adequate.

The phase path length in an ionized medium is smaller than that in vacuum. The path length reduction, ΔP, due to the ionosphere is given by

$$\Delta P = \int_g ds - \int_p \mu ds = \int_g (1 - \mu) ds + \left[\int_g \mu ds - \int_p \mu ds \right] \qquad (6)$$

in which the subscripts g and p refer to integrals along the geometric and refracted paths, respectively. The last two terms, in the square brackets, represent the correction for refraction. If refraction is neglected and a linearized expression for μ is employed, one obtains

$$\Delta P = \int_g \frac{e^2 n}{4\pi^2 m \epsilon_0 f^2} ds \approx \frac{40.3}{f^2} \int_g n ds \equiv \Delta P_0 \qquad (7)$$

where ΔP_0 is the first order term for phase path reduction in meters, e and m are the charge and mass of the electron, ϵ_0 is the permittivity of free space and f is the frequency in Hz. The ionospheric Doppler shift is then

$$f_I = \frac{1}{\lambda} \frac{d}{dt} (\Delta P) \approx \frac{40.3}{cf} \frac{d}{dt} \int_g n \, ds \equiv f_{I_0} \qquad (8)$$

in which the approximation gives the first order contribution to f_I. Ross [1965] has shown how the full value of f_I can be related to the first order term f_{I_0} (and similarly for polarization rotation measurements). His method requires an estimate of the ionospheric layer shape, although the correction is not particularly sensitive to the exact shape assumed. All of the data used in this paper, both ionospheric Doppler shift, f_I, and polarization rotation measurement, have included the second order corrections of Ross. In this way, all integrals can be taken along the geometric ray path.

Briefly summarizing the procedure again, f_I is calculated from equation (4) and then related to f_{I_0} with Ross's second order equations. This value is inserted in equation (8) to give the rate change of electron content.

The determination of $d\Omega/dt$ is straight forward. Due to the spinning of the satellite, the plane of polarization of the wave radiated from the dipole antenna rotates with an angular frequency $2\pi f_s$. If the Faraday roation angle, Ω, changes with time, then the plane of polarization of the wave at the receiver rotates with an angular frequency $2\pi f_s + \frac{d\Omega}{dt}$. Thus, the amplitude of the signal received with a linear array shows cyclic variations with consecutive minima separated by a time interval $T_0/2$ where

$$T_0 = \left(f_s + \frac{1}{2\pi} \cdot \frac{d\Omega}{dt}\right)^{-1}$$

The time interval between minima is scaled from graphic records of the 40 MHz signal amplitude and the value of $\frac{d\Omega}{dt}$ is obtained from

$$\frac{1}{m}\frac{d\Omega}{dt} = 2\pi\left(\frac{1}{mT_0} - \frac{1}{mT_s}\right) \quad \text{radians sec}^{-1}$$

where m is any convenient integral number of total fades. The integer is increased to minimize scaling errors, consistent with the desired time resolution.

III - METHOD OF ANALYSIS

In the preceding section it was shown how the raw data received from the satellite were processed to yield the time rates of change of the slant electron content, $\frac{dI}{dt}$ (from the differential Doppler experiment) and of the Faraday rotation angle, $\frac{d\Omega}{dt}$ (from the Faraday experiment). In this section these two quantities will be used to derive the local electron concentration at the satellite.

It should be noted that the electron concentration, n, is a function of position and of time, i.e., $n = n(h,x,y,t)$ where h is the height and x and y denote directions, respectively, in and normal to the plane of incidence. The zenithal angle, φ, is a function of h and x or, more conveniently, of h and φ_o where φ_o is the zenithal angle at the observer. The rate of change of slant electron content is therefore

$$\frac{dI}{dt} = \frac{d}{dt}\int_0^S n\,ds = \frac{d}{dt}\int_0^{h_S} n \sec\varphi\, dh =$$

$$= n_S \sec\varphi_S \frac{dh_S}{dt} + \frac{d\varphi_o}{dt}\int_0^{h_S} n\frac{\partial}{\partial\varphi_o}(\sec\varphi)\, dh + \int_0^{h_S}\frac{\partial n}{\partial t}\sec\varphi\, dh +$$

$$+ \int_0^{h_S}\frac{dx}{dt}\cdot\frac{\partial n}{\partial x}\sec\varphi\, dh + \int_0^{h_S}\frac{dy}{dt}\cdot\frac{\partial n}{\partial y}\sec\varphi\, dh \qquad (9)$$

Equation (9), above, is exactly equivalent to equation (2) of the paper by Ross, Garriott, Mendonça and da Rosa, [1968].

If the motion of the satellite were entirely along the ray path, then $\frac{d\varphi_o}{dt} = \frac{dx}{dt} = \frac{dy}{dt} = 0$. If, in addition, no temporal changes occurred $\left(\frac{\partial n}{\partial t} = 0\right)$, then equation (9) would yield

$$n_S = \frac{dI/dt}{\sec\varphi_S \; dh_S/dt}$$

Since the above conditions generally do not hold, it becomes necessary to take into account the four last terms on the right hand side of equation (9). This can be accomplished by using the observed Faraday rotation angle.

An equation similar to equation (9) will be obtained for the rate of Faraday rotation, $d\Omega/dt$. It will be found that this equation has seven terms, five of which are analogous to the five terms of the expression for dI/dt. Of these, the term containing n_S is much less important than in the Doppler case, owing to the very small magnetic flux density at great altitudes. The remaining four terms will be of nearly equal importance to their corresponding terms in equation (9). Therefore, a proper combination of Faraday rotation and ionospheric Doppler shift measurements can result in a near cancellation of the four last terms in equation (9), without eliminating the desired term containing n_S. The sixth and seventh term in the expression for $d\Omega/dt$ must be considered separately.

The Faraday rotation angle, Ω is

$$\Omega = Q_F \int_0^{h_S} n \sec \varphi \, B_L \, dh \tag{10}$$

$$Q_F \equiv \frac{2.36 \times 10^4}{f^2} \tag{11}$$

Here, f is the frequency of the received signal, in Hz, and B_L is the component of the geomagnetic flux density along the ray path in weber m^{-2}. B_L is a function of position, i.e., $B_L = B_L(h,x,y)$.

A "true mean longitudinal geomagnetic flux density", $\langle B_L \rangle$, is given by the ratio:

$$\langle B_L \rangle \equiv \frac{\int_0^{h_S} n \sec \varphi \, B_L \, dh}{\int_0^{h_S} n \sec \varphi \, dh} \tag{12}$$

The value of $\langle B_L \rangle$ depends only on the shape of the electron concentration profile and not on the magnitude of the concentration.

Since the exact shape of the profile is unknown, $\langle B_L \rangle$ is known only approximately.

$$\langle B_L \rangle \equiv \langle B_L \rangle_E + \delta \langle B_L \rangle \tag{13}$$

Here $\langle B_L \rangle_E$ is the best estimate of the mean flux density and $\delta\langle B_L \rangle$ is its unknown deviation from the true value.

Taking the time derivative of Ω and dividing by $Q_F \langle B_L \rangle_E$ one obtains the expression

$$\frac{1}{Q_F \langle B_L \rangle_E} \cdot \frac{d\Omega}{dt} = n_S \sec \varphi_S \frac{B_{L_S}}{\langle B_L \rangle_E} \frac{dh_S}{dt} + \frac{d\varphi_o}{dt} \int_0^{h_S} n \frac{\partial}{\partial \varphi_o} (\sec \varphi) \frac{B_L}{\langle B_L \rangle_E} dh +$$

$$+ \int_0^{h_S} \frac{\partial n}{\partial t} \sec \varphi \frac{B_L}{\langle B_L \rangle_E} dh + \int_0^{h_S} \frac{dx}{dt} \cdot \frac{\partial n}{\partial x} \sec \varphi \frac{B_L}{\langle B_L \rangle_E} dh +$$

$$+ \int_0^{h_S} \frac{dy}{dt} \cdot \frac{\partial n}{\partial y} \sec \varphi \frac{B_L}{\langle B_L \rangle_E} dh + \int_0^{h_S} \frac{dx}{dt} \cdot \frac{\partial B_L}{\partial x} n \sec \varphi \frac{dh}{\langle B_L \rangle_E} +$$

$$+ \int_0^{h_S} \frac{dy}{dt} \cdot \frac{\partial B_L}{\partial y} n \sec \varphi \frac{dh}{\langle B_L \rangle_E} \tag{14}$$

which is the result analogous to equation (9).

Subtracting equation (14) from equation (9) one obtains

$$\frac{dI}{dt} - \frac{1}{Q_F \langle B_L \rangle_E} \cdot \frac{d\Omega}{dt} = n_S V_{eff} + \frac{d\varphi_o}{dt} \int_0^{h_S} n \frac{\partial}{\partial \varphi_o} (\sec \varphi) \Psi \, dh +$$

$$+ \int_0^{h_S} \frac{\partial n}{\partial t} \sec \varphi \Psi \, dh + \int_0^{h_S} \frac{dx}{dt} \cdot \frac{\partial n}{\partial x} \sec \varphi \Psi \, dh +$$

$$+ \int_0^{h_S} \frac{dy}{dt} \cdot \frac{\partial n}{\partial y} \sec \varphi \Psi \, dh - \int_0^{h_S} \frac{dx}{dt} \cdot \frac{\partial B_L}{\partial x} n \sec \varphi \frac{dh}{\langle B_L \rangle_E} -$$

$$- \int_0^{h_S} \frac{dy}{dt} \cdot \frac{\partial B_L}{\partial y} n \sec \varphi \frac{dh}{\langle B_L \rangle_E} \qquad (15)$$

where

$$V_{eff} \equiv \sec \varphi_S \frac{dh_S}{dt} \left(1 - \frac{\bar{B}_{L_S}}{\langle B_L \rangle_E} \right)$$

and

$$\Psi \equiv 1 - \frac{B_L}{\langle B_L \rangle_E}$$

Equation (15) permits the calculation of n_S:

$$n_S = \frac{1}{V_{eff}}\left[\frac{dI}{dt} - \frac{1}{Q_T\langle B_L\rangle_E}\cdot\frac{d\Omega}{dt} - \frac{d\varphi_o}{dt}\int_0^{h_S} n\,\frac{\partial}{\partial\varphi_o}(\sec\varphi)\,\Psi\,dh - \right.$$

$$- \int_0^{h_S}\frac{\partial n}{\partial t}\sec\varphi\,\Psi\,dh$$

$$- \int_0^{h_S}\frac{dx}{dt}\cdot\frac{\partial n}{\partial x}\sec\varphi\,\Psi\,dh - \int_0^{h_S}\frac{dy}{dt}\cdot\frac{\partial n}{\partial y}\sec\varphi\,\Psi\,dh +$$

$$\left. + \int_0^{h_S}\frac{dx}{dt}\cdot\frac{\partial B_L}{\partial x}\,n\sec\varphi\,\frac{dh}{\langle B_L\rangle_E} + \int_0^{h_S}\frac{dy}{dt}\cdot\frac{\partial B_L}{\partial y}\,n\sec\varphi\,\frac{dh}{\langle B_L\rangle_E}\right] \qquad (16)$$

The six integrals on the right hand side of equation (16) merit discussion. Consider first the term containing $\frac{\partial}{\partial t}(\sec\varphi)$. Assume the shape of the sec φ profile does not change with time, i.e., $\frac{\partial}{\partial t}(\sec\varphi) = \beta_1 \sec\varphi$ where β_1 may vary with time but not with height. The integral may then be written as

$$\int_0^{h_S} n\,\frac{\partial}{\partial t}(\sec\varphi)\,\Psi\,dh = \beta_1\int_0^{h_S} n\sec\varphi\,dh -$$

$$- \beta_1\int_0^{h_S} n\sec\varphi\,\frac{B_L}{\langle B_L\rangle_E}\,dh = 0$$

as can be seen by referring to the definition of $\langle B_L\rangle$ in equation (12).

The shape of the sec φ profile cannot be exactly preserved when the satellite has any angular motion with respect to the observer. However, if a plausible electron concentration profile is adopted, it is possible

to compute

$$\int_0^{h_S} n \frac{\partial}{\partial t} (\sec \varphi) \Psi \, dh$$

and it is found that this integral makes only a small contribution to the value of n_S.

In a similar fashion, since the value of sec $\varphi(h,x,y)$ and of $B_L(h,x,y)$ can be determined with good precision from the known positions of observer and satellite, it is possible to obtain values for the last two integrals of equation (16) once a reasonable concentration profile is adopted.

The remaining three integrals in equation (16) cannot be evaluated from the available data and their contributions will be treated as uncertainties in the value of n_S. It should, nevertheless, be noted that if the shape of the n-profile is time-independent, i.e., if $\frac{\partial n}{\partial t} = \beta_2 n$, then, just as in the case of the $\frac{\partial}{\partial t}(\sec \varphi)$ term, the integral is zero. Thus, for example, the temporal term contributes uncertainty to the computed value of electron concentration only through changes in the profile shape. The errors introduced by neglecting these integrals in equation (16) are discussed, together with other uncertainties, in the next section.

All results discussed in this paper were obtained from equation (17) below:

$$n_S = \frac{1}{V_{eff}} \left[\frac{dI}{dt} - \frac{1}{Q_F \langle B_L \rangle_E} \cdot \frac{d\Omega}{dt} - \frac{d\varphi_o}{dt} \int_0^{h_S} n \frac{\partial}{\partial \varphi_o} (\sec \varphi) \Psi \, dh + \right.$$

$$\left. + \int_0^{h_S} \frac{dx}{dt} \cdot \frac{\partial B_L}{\partial x} n \sec \varphi \frac{dh}{\langle B_L \rangle_E} + \int_0^{h_S} \frac{dy}{dt} \cdot \frac{\partial B_L}{\partial y} n \sec \varphi \frac{dh}{\langle B_L \rangle_E} \right] \qquad (17)$$

The value of $\langle B_L \rangle$ is estimated by assuming that the plasmasphere consists of two parts:

1 - an ionosphere (below the level at which H^+ predominates) with an α-Chapman distribution characterized by h_{max},

the height of the peak concentration, and by a height-dependent temperature, T(h).

2 - a protonosphere characterized by a peak height, h_x, above which the concentration decays exponentially with a height-dependent scale height, H_H, appropriate for a constant temperature proton layer and, below which, the ionization decays in accordance to an α-Chapman layer with scale height equal to $1/7\ H_H$.

The ratio between the proton concentration at h_x and the oxygen ion concentration at h_{max} is defined as γ. Under the above assumptions

$$\langle B_L \rangle = \frac{\int_0^{h_S} N_{O^+}(h)\ \sec\varphi\ B_L\ dh + \gamma \int_0^{h_S} N_{H^+}(h)\ \sec\varphi\ B_L\ dh}{\int_0^{h_S} N_{O^+}(h)\ \sec\varphi\ dh + \gamma \int_0^{h_S} N_{H^+}(h)\ \sec\varphi\ dh} \qquad (18)$$

where $N_{O^+}(h)$ and $N_{H^+}(h)$ are the normalized electron concentration function conforming to the above description of the plasmasphere.

The appropriate parameters for the plasmaspheric models used in the computations were mostly obtained from the Thomson scatter results of Evans [1967]. These results are presented as monthly averages covering the same period of the OGO-I observations and, although referring to the ionosphere above Millstone Hill, Massachusetts, were assumed to be applicable to Stanford, California.

The value of h_{max} at the time of interest -- aroung 1100 LMT -- in October 1964 was approximately 230 km. A slightly lower value prevailed in November and a somewhat higher one in December.

The plasma temperature profile adopted for the computation of the electron concentration model was a piecewise linear approximation to the average of Evans' electron and ion temperatures. Figure 1 shows the measured average daytime ion and electron temperature for October 1964 as

well as the resulting plasma temperature. The electron temperature was arbitrarily extrapolated above the maximum measurement height of 600 km under the assumption that this temperature becomes height-independent near 1000 km. The dashed line superposed on the plasma temperature was assumed to be equal to 355 K at 120 km, equal to 1000 K at 220 km and equal to 3000 K at 825 km and above. Linear interpolation between these values was used.

The protonospheric scale height H_H was taken as the height-dependent scale height appropriate for a constant temperature neutral hydrogen layer. The plasma profile was computed using $2H_H$.

The value of h_x was taken as 1000 km and the value of γ as 1/100 consistent with Alouette I results [Thomas, Rycroft, Colin and Chan, 1965].

IV - UNCERTAINTIES

It was shown in section II how the quantities dI/dt and $d\Omega/dt$ were extracted from the raw data and, in section III, how these quantities were used in the determination of n_S, the local electron concentration at the satellite. In view of the important role the error analysis plays in the interpretation of the measurements, the question of uncertainties will be discussed in this section, prior to the presentation of the results in section V.

The values of electron concentration have uncertainties which fall, broadly, into five categories:

1. δn_{S_1}: uncertainties resulting from errors in the measurement of dI/dt and $d\Omega/dt$.

2. δn_{S_2}: uncertainties resulting from the approximate nature of the ionospheric models used in the data reduction. This affects the value of $\langle B_L \rangle_E$ and of the three last integrals in equation (17).

3. δn_{S_3}: uncertainties resulting from neglecting the temporal shape changes in the electron concentration profile.

4. δn_{S_4} : uncertainties resulting from neglecting horizontal gradients of ionization,

5. δn_{S_5} : uncertainties due to the errors in evaluating the three integrals in equation (17).

A - Uncertainties in the measurement of dI/dt and dΩ/dt

The principal uncertainty in the measurement of dI/dt and dΩ/dt results from errors in data scaling.

From equations (4) and (8)

$$\frac{dI}{dt} \approx \frac{cf}{40.3}\left(f_b - f_S\right) \equiv \frac{1}{Q_D}\left(f_b - f_S\right)$$

The spin frequency, f_s, is known with a precision much better than 1 part in 1000. Its contribution to an uncertainty in dI/dt is, thus

$$\delta \frac{dI}{dt} < \frac{f_s}{Q_D} \times 10^{-3} \approx 2.5 \times 10^{10} \text{ el.m}^{-2}\text{sec}^{-1}$$

The resulting uncertainty in n_S is (c.f. equation (17))

$$\delta n_S = \frac{\delta \frac{dI}{dt}}{V_{eff}} < 5 \text{ el.cm}^{-3} \qquad (19)$$

which is entirely negligible.

In the above example, as in all cases in this section, V_{eff} was taken as 5000 m sec^{-1}, typical for all OGO-I passes considered in this paper.

To determine the frequency, f_b of the Doppler beat, the corresponding period is scaled from a chart (a 2.5 mm sec^{-1} speed was used in all records).

The uncertainty in the time measurement can, conservatively, be estimated as 0.5 seconds. The value of f_b is then

$$f_b = \frac{m}{mT \pm 0.5}$$

and

$$\delta f_b = \frac{0.5}{m\,T^2} \qquad \text{sec}^{-1}$$

Here m is an integer representing the number of cycles counted and T is the period of the differential Doppler beat. Thus mT is the integration time. The period T of the differential Doppler beat seldom becomes smaller than 8 seconds. Using this value for T and considering 60 seconds integration time, the uncertainty in f_b is 10^{-3} sec^{-1} resulting in a $\delta \frac{dI}{dt}$ of some 3×10^{11} el.m^{-2} sec^{-1} and a corresponding uncertainty in n_s of about 60 el.cm^{-3}. With a five minute integration time this uncertainty in the local electron concentration is, of course, reduced to 12 el.cm^{-3}, which is also negligible.

Referring back to section II, one can see that

$$\frac{1}{m}\frac{d\Omega}{dt} = 2\pi\left(\frac{1}{mT_0} - \frac{1}{mT_s}\right) \text{ rad. sec}^{-1}$$

where both T_0 and T_s are of the order of 12 seconds and mT_s is the integration time.

Assuming the same 0.5 second uncertainty in the determination of the time of a given fade, the error in $d\Omega/dt$ is

$$\delta \frac{d\Omega}{dt} = \frac{\pi}{mT_0^{\,2}}$$

With 60 second integration time $\delta \frac{d\Omega}{dt} \approx 4 \times 10^{-3}$ rad.sec^{-1}. The corresponding error in n_S is

$$\delta n_{S_1} = \frac{\delta \frac{d\Omega}{dt}}{V_{eff} Q_F \langle B_L \rangle} \approx 1500 \text{ el.cm}^{-3} \qquad (20)$$

when the value of $\langle B_L \rangle = 3 \times 10^{-5}$ weber m^{-2} is used.

This is a very substantial uncertainty and, to reduce it, the calculations in this paper were made with integration times of 5 minutes. With such an integration time δn_{S_1}, due to scaling errors in $d\Omega/dt$, is about 300 el.cm^{-3}. This is one of the most important sources of error in the whole analysis.

B - Uncertainties due to errors in $\langle B_L \rangle$

It was pointed out in section III that there is an uncertainty, $\delta\langle B_L \rangle$, in the value of the mean longitudinal geomagnetic flux density $\langle B_L \rangle_E$ used in the calculations. This uncertainty stems from the incomplete knowledge of the exact shape of the electron concentration profile. In this sub-section the magnitude of $\delta\langle B_L \rangle$ will be estimated and the resulting error in n_S will be determined. Neglecting, for the moment, the relatively small contribution from the integrals in equation (17), the local electron concentration is given by

$$n_S = \frac{\frac{dI}{dt} - \frac{1}{Q_F} \cdot \frac{d\Omega}{dt} \cdot \frac{1}{\langle B_L \rangle_E}}{\sec \varphi \frac{dh_S}{dt} \left(1 - \frac{B_{L_S}}{\langle B_L \rangle_E} \right)} \qquad (21)$$

The effect on n_S of small changes in $\langle B_L \rangle_E$ can be determined by taking the derivative of n_S with respect to $\langle B_L \rangle_E$ and equating the finite increments (δn_S, $\delta\langle B_L \rangle_E$) to the corresponding infinitesimal increments dn_S and $d\langle B_L \rangle_E$. The resulting expression for δn_S is

$$\delta n_{S_2} = \left(\frac{\frac{dI}{dt}}{\sec \varphi_S \frac{dh_S}{dt}} - n_S \right) \frac{\delta \langle B_L \rangle_E}{\langle B_L \rangle_E - B_{L_S}} \approx \frac{d\Omega/dt}{Q_F V_{eff} \langle B_L \rangle_E} \cdot \frac{\delta \langle B_L \rangle_E}{\langle B_L \rangle_E - B_{L_S}} \quad (22)$$

In order to use equation (22), it is necessary to estimate $\delta\langle B_L \rangle$. This is done by inquiring what is the effect on $\langle B_L \rangle_E$ of changing the parameters of the plasmaspheric model. To accomplish this, a slight simplification was introduced in the model used in the actual computation of n_S (described in section III): the scale height in the lower ionosphere was maintained constant.

Then

$$\delta\langle B_L \rangle = \frac{\partial \langle B_L \rangle}{\partial h_{max}} dh_{max} + \frac{\partial \langle B_L \rangle}{\partial H_0} dH_0 + \frac{\partial \langle B_L \rangle}{\partial h_x} dh_x +$$

$$+ \frac{\partial \langle B_L \rangle}{\partial H_H} dH_H + \frac{\partial \langle B_L \rangle}{\partial \gamma} d\gamma \quad (23)$$

where h_{max} and h_x are the heights of the peaks in, respectively, the ionized oxygen and the proton layers; H_0 and H_H are, respectively, the scale heights of neutral oxygen and hydrogen, and γ has the definition given in section III.

Using equation (18), values of $\langle B_L \rangle$ were computed for various combinations of the five parameters and the partial derivatives were calculated. Table 2 presents a summary of the results.

Table 2

VALUES OF THE PARTIAL DERIVATIVES OF $\langle B_L \rangle$

Constant Scale height. 12 Dec 64 18:45
OGO-I (Seen from Stanford)
Position of the satellite: 10055 km, 207.5°E, 28.2°N
Azim: 258.9° Elev. 47.9°
h_x = 1000 km

h_{max} (km) ↓	H_H = 800 km			H_H = 1400 km		← H_0 (km)
	40	80		40	80	
190	- 12.0	- 16.0		- 11.0	- 16.0	$\frac{\partial \langle B_L \rangle}{\partial h_{max}}$
	- 11.0	- 15.0		- 11.0	- 14.0	
310	- 10.0	- 14.0		- 10.0	- 14.0	
	- 9.0	- 13.0		- 9.0	- 13.0	weber m^{-2} x 10^{12}
180	41	7		43	19	$\frac{\partial \langle B_L \rangle}{\partial H_0}$
	72	20		107	39	
320	15	0		45	11	
	46	14		83	30	weber m^{-2} x 10^{12}
180	- 0.6	- 0.4		- 0.7	- 0.4	$\frac{\partial \langle B_L \rangle}{\partial h_x}$
	- 1.1	- 0.7		- 1.4	- 0.7	
320	- 0.6	- 0.4		- 0.9	- 0.4	
	- 1.1	- 0.7		- 1.4	- 0.9	weber m^{-2} x 10^{12}
180	- 4.1	- 2.4		- 3.1	- 1.8	$\frac{\partial \langle B_L \rangle}{\partial H_H}$
	- 7.5	- 4.5		- 3.9	- 2.5	
320	- 4.3	- 2.4		- 3.0	- 1.6	
	- 7.0	- 3.9		- 3.6	- 2.4	weber m^{-2} x 10^{12}
180	-210	-122		-313	-196	$\frac{\partial \langle B_L \rangle}{\partial \gamma}$
	-173	-103		-236	-122	
320	-193	-109		-289	-181	
	-158	- 99		-207	-112	weber m^{-1}

Top line in the body of the table: $\gamma = 1/100$
Bottom line : $\gamma = 1/50$

Table 3 below indicates the most probable value for the model parameters as well as the estimated uncertainties.

Table 3

Model Parameters used in the Calculation of $\langle B_L \rangle$

Parameter	Most probable value	Uncertainty	Units
h_{max}	230	± 20	km
H_0	60	± 10	km
h_x	1000	± 400	km
H_H	2550	± 500	km
γ	0,01	± 0,003	--

Combining the uncertainties of table 3 with the appropriate partial derivatives in table 2, one obtains

Table 4

Uncertainties in $\langle B_L \rangle$

Uncertainty due to	$\delta \langle B_L \rangle$ (w m^{-1} x 10^6)
δh_{max}	0.30
δH_0	0.31
δh_x	0.23
δH_H	1.25
$\delta \gamma$	0.75

The total uncertainty in $\delta \langle B_L \rangle$ is most probably the square root of the sum of the squares of the individual uncertainties. Thus

$$\delta \langle B_L \rangle = 1.53 \times 10^{-6} \text{ wb } m^{-2}$$

The uncertainty in the height h_x, a quantity that is very poorly known, has a negligible effect on the results. The protonospheric parameters, H_H and γ, have a much more significant effect on the errors in the analysis than do the parameters h_{max} and H_0.

Having extimated a value of $\delta\langle B_L\rangle$, the corresponding uncertainty associated with each calculated value of electron concentration can be computed from equation (22). However, to estimate the order of magnitude of the uncertainties being discussed, it is more convenient to refer back to equation (21) introducting a simplification based on the fact that $B_{L_S} \ll \left(\langle B_L\rangle_E\right)$.

$$n_S \approx \frac{\frac{dI}{dt} - \frac{1}{Q_F} \cdot \frac{d\Omega}{dt} \cdot \frac{1}{\langle B_L\rangle_E}}{\sec \varphi_S \frac{dh_S}{dt}}$$

Thus

$$\delta n_{S_2} \approx \frac{\frac{d\Omega}{dt} \cdot \delta \langle B_L\rangle}{Q_F \sec \varphi_S \frac{dh_S}{dt} \langle B_L\rangle_E^2} \approx 2.2 \times 10^4 \frac{d\Omega}{dt} \quad el.cm^{-3} \qquad (24)$$

in which $\sec \varphi_S \frac{dh_S}{dt}$ was taken as 5000 m sec^{-1} as mentioned before. It is seen that the uncertainty is proportional to the rate of change of the Faraday rotation angle. A representative value of this rate is 0.01 rad. sec^{-1} yielding an uncertainty of 220 $el.cm^{-3}$.

The effect of uncertainties in $\langle B_L\rangle_E$ on the last two integrals of equation (17) will be discussed in subsection E.

C - Uncertainties due to the neglect of temporal variations in the shape of the electron concentration profile

The electron concentration model used in this analysis was described in section III. In order to estimate the errors resulting from the neglect of the integral containing $\partial n/\partial t$ in equation (16), the somewhat simpler model below will be used.

$$n = n_{max} \left[N_{O^+}(h) + \gamma N_{H^+}(h)\right] \qquad (25)$$

$$N_{O^+} \equiv \exp\left[\frac{1}{2}(1 - z - e^{-z})\right] \tag{26}$$

$$z \equiv \frac{h - h_{max}}{H_O} \tag{27}$$

$$N_{H^+} = 0 \qquad h < h_x \tag{28}$$

$$N_{H^+} = \exp\left[\frac{R_o}{H_{H^+}}\left(\frac{R_o}{R} - 1\right)\right] \tag{29}$$

where

h is the height variable

h_{max} is the height of the F2 peak

H_O is the scale height of the neutral monoatomic oxygen molecule

ρ is the radius of earth

$R \equiv \rho + h$

$R_o \equiv \rho + h_x$

H_{H^+} is the scale height of the protons at the height h_x

The uncertainty in n_S due to $\partial n/\partial t$ is (c.f. equation (16)):

$$\delta n_{S_3} = \frac{1}{V_{eff}} \int_0^{h_S} \frac{\partial n}{\partial t} \sec \varphi \left(1 - \frac{B_L}{\langle B_L \rangle_E}\right) dh =$$

$$\frac{1}{V_{eff}} \left[\int_0^{h_S} \frac{\partial n}{\partial t} \sec \varphi \, dh - \frac{1}{\langle B_L \rangle} \int_0^{h_S} \frac{\partial n}{\partial t} \sec \varphi \, B_L \, dh\right] =$$

$$\left[\frac{dn_{max}}{dt} \int_0^{h_S} \left(N_{O^+} + \gamma N_{H^+}\right) \sec \varphi \, dh - \frac{dn_{max}}{dt} \cdot \frac{1}{\langle B_L \rangle} \int_0^{h_S} \left(N_{O^+} + \gamma N_{H^+}\right) \sec \varphi \, B_L \, dh + \right.$$

$$\left. + n_{max} \int_0^{h_S} \frac{d}{dt}\left(N_{O^+} + \gamma N_{H^+}\right) \sec \varphi \left(1 - \frac{B_L}{\langle B_L \rangle}\right) dh\right] \frac{1}{V_{eff}} =$$

$$\frac{n_{max}}{V_{eff}} \int_0^{h_S} \frac{d}{dt}\left(N_{O^+} + \gamma N_{H^+}\right) \sec \varphi \left(1 - \frac{B_L}{\langle B_L \rangle}\right) dh$$

It can be seen here that, as pointed out in the previous section, it is only the change in the shape of the electron concentration profile that makes a contribution to the uncertainty.

By noting that N_{O^+} is a function of h_{max} and H_O, and that N_{H^+} is a function of h_x and H_{H^+}, the uncertainty can be written as

$$\delta n_{S_3} = \frac{n_{max}}{V_{eff}} \left\{ \int_0^{h_S} \frac{N_{O^+}}{2H_O} (1 - e^{-z}) \left(\frac{dh_{max}}{dt} + z \frac{dH_O}{dt} \right) \sec \varphi \left(1 - \frac{B_L}{\langle B_L \rangle} \right) dh + \right.$$

$$+ \gamma \int_0^{h_S} \frac{N_{H^+}}{H_{H^+}} \left[\left(\frac{2R_o}{R} - 1 \right) \frac{dh_x}{dt} - \frac{R_o}{H_{H^+}} \left(\frac{R_o}{R} - 1 \right) \frac{dH_{H^+}}{dt} \right] \sec \varphi \left(1 - \frac{B_L}{\langle B_L \rangle} \right) dh +$$

$$\left. + \frac{d\gamma}{dt} \int_0^{h_S} N_{H^+} \sec \varphi \left(1 - \frac{B_L}{\langle B_L \rangle} \right) dh \right\} \qquad (30)$$

Using the above equation and the estimate of the maximum values of the rate of change of the different parameters (see Table 5) the uncertainty in the local electron concentration due to the neglect of temporal variations can be computed. It must be pointed out that all the OGO-I data were obtained near midday when one may expect all temporal changes to be a minimum.

Although it is simple to perform the numerical computations indicated by equation (30), it is not easy to estimate "a priori" the magnitude of the uncertainty given by that equation. Numerical calculations indicate that the uncertainty is quite small and that the dominant contribution comes from the term involving $d\gamma/dt$. If one disregards the other terms, then it becomes possible to estimate the resulting δn_S.

If $\frac{dh_{max}}{dt} = \frac{dH_O}{dt} = \frac{dh_x}{dt} = \frac{dH_{H^+}}{dt} = 0$ then, from equation (30),

$$\delta n_{S_3} < \frac{n_{max}}{V_{eff}} \cdot \frac{d\gamma}{dt} \int_{h_x}^{\infty} N_{H^+} \sec \varphi \, dh$$

Table 5

Estimate of the maximum rate of change of the electron concentration model parameters		
	km/hr	m/s
$\frac{dh_{max}}{dt}$	7.2	2
$\frac{dH_0}{dt}$	7.2	2
$\frac{dh_x}{dt}$	72	20
$\frac{dH_{H^+}}{dt}$	144	40
$\frac{dv}{dt}$	3×10^{-7} sec^{-1} (change from 1/90 to 1/100 in one hour)	

Since $N_{H^+} \approx e^{-\frac{h}{H^+}}$ the integral is less than

$$\int_{h_x}^{\infty} N_{H^+} \sec \varphi \, dh \approx H^+ \langle \sec \varphi \rangle \, e^{-\frac{h_x}{H^+}} \approx 10^7 \text{ m}^{-2}$$

Here $\langle \sec \varphi \rangle$ was taken equal to 1, h_x = 1000 km and H^+ = 6000 km. Using $n_{max} = 3 \times 10^5$ el.cm^{-3}, $\frac{d\gamma}{dt} = 3 \times 10^{-7}$ sec^{-1} and V_{eff} = 5000 m sec^{-1}, one obtains

$$\delta n_{S_3} < 100 \text{ cm}^{-3}$$

D - Uncertainties due to the neglect of horizontal ionization gradients

The second and third integrals in equation (16) represent the effect of horizontal gradients of ionization and give rise to the uncertainty δn_{S_4}.

$$\delta n_{S_4} = \frac{1}{V_{eff}} \left(\int_0^{h_S} \frac{dx}{dt} \frac{\partial n}{\partial x} \sec \varphi \, \Psi \, dh + \int_0^{h_S} \frac{dy}{dt} \frac{\partial n}{\partial y} \sec \varphi \, \Psi \, dh \right) =$$

$$= \frac{1}{V_{eff}} \left(\frac{d\varphi_o}{dt} \int_0^{h_S} \frac{\partial n}{\partial x} r \sec^2 \varphi \, \Psi \, dh + \sin \varphi_o \frac{d\alpha}{dt} \int_0^{h_S} \frac{\partial n}{\partial y} r \sec \varphi \, \Psi \, dh \right) \quad (31)$$

where r is the distance from the observer and α is the azimuth of the satellite.

If one assumes that the gradients of concentration in and normal to the plane of incidence have the same value and that they are proportional to the concentration itself, i.e., if $\frac{\partial n}{\partial x} = \frac{\partial n}{\partial y} = \beta_3 n$ where β_3 does not depend on height, then

$$\delta n_{S_4} = \frac{\beta_3}{V_{eff}} \int_0^{h_S} n \, \Psi \, r \sec \varphi \left(\left| \frac{d\varphi_o}{dt} \sec \varphi \right| + \left| \frac{d\alpha}{dt} \sin \varphi_o \right| \right) dh \quad (32)$$

The magnitude of this uncertainty is critically dependant on the horizontal motion of the satellite, a quantity that varies greatly from pass to pass and also varies substantially throughout a given pass. The absolute value symbols in equation (32) assure that δn_{S_4} always corresponds to a "worst case" condition where the effects of the x- gradient always add to the effects of the y-gradient.

The values of δn_{S_4} were computed for each data point using equation (32), assuming that the gradients were of 1% of the concentration in 100 km. These were the values adopted by Ross et al. [1968]. A typical value of this uncertainty is about 300 el.cm^{-3}, although in some passes the uncertainty may reach twice the figure quoted. This cause of errors is a very important one.

E - Uncertainties due to errors in evaluating the integrals in equation (17)

The three integrals in equation (17) involve the weighted means of the quantities $\frac{\partial}{\partial\varphi_o}(\sec\varphi)$, $\frac{dx}{dt}\cdot\frac{\partial B_L}{\partial x}\sec\varphi$, and $\frac{dy}{dt}\cdot\frac{\partial B_L}{\partial y}\sec\varphi$. These quantities themselves are known with good precision but their weighting factor must be estimated from assumed ionospheric models. The weighting factor for the first mean is $n\Psi$ and for the last two is n.

As pointed out in section III, the integral containing $\frac{\partial}{\partial\varphi_o}(\sec\varphi)$ has a small value compared with that of the remaining terms in the brackets of equation (17) and will contribute only insignificantly to the uncertainties in n_S.

Depending on the values of $\frac{dx}{dt}$ and $\frac{dy}{dt}$, the two last integrals in equation (17) may be of the same order of magnitude as

$$\frac{dI}{dt} - \frac{1}{Q_F\langle B_L\rangle_E}\cdot\frac{d\Omega}{dt}$$

For this reason only runs with small angular motion of the satellite can be used for the computation of local electron concentration. This imposes a severe restriction on the number of useful passes. The errors in estimating the integrals under discussion come from two sources: a) errors in estimating the magnitude of n, i.e., errors in the determination of n_{max} and b) uncertainties in the shape of the assumed n-profile.

Ionograms permit a good determination of n_{max}. Typically, the critical frequency during the runs was some 5 MHz and its value could be scaled within ± 100 kHz yielding an uncertainty of 4% in n_{max}. Due to the fact that the ionosonde at Stanford was not at the subionospheric point of the ray path from satellite to receiving station, the actual uncertainty in n_{max} at the point of interest was somewhat larger than the value quoted above. In addition using a technique similar to the one described in subsection B, it was found that the uncertainties in profile shape would introduce errors of about 6% in the value of the integrals. An aggregate error of 10% was assumed in the calculations.

The uncertainties originating from the individual causes discussed here were computed for each value of electron concentration obtained from the experiment and a total uncertainty (square root of the sum of the squares of each uncertainty) was assigned to each value.

V - RESULTS

The results obtained with the OGO-I beacon experiment are presented in this section. The data were analyzed using the technique described in the previous sections. The electron concentrations were computed from equation (17). For each datum, an independent value of $\langle B_I \rangle$ was calculated using equation (18) and employing the model parameters shown in Table 3. The uncertainties due to scaling errors were computed from equation (20) and those due to errors in $\langle B_L \rangle$ were calculated from equation (22). The errors due to the neglect of the temporal changes in the shape of the electron concentration profile were obtained from equation (30) and were, in general, found to be negligible. Equation (31) yielded the uncertainties due to the neglect of horizontal ionization gradients. The errors resulting from the inaccuracy in the determination of the two last integrals in equation (17) were assumed to be 10% of the value of the best estimate of these integrals.

All data used in this work were collected during the early life of OGO-I while the perigee was still low. The rapid growth in perigee height caused the satellite to be visible only when its altitude was so high that most of the runs started with the beacon already outside the plasmapause.

Plots of electron concentration at the satellite versus the height of the spacecraft are shown in Figure 2. All the data were taken at Stanford around 11:00 PST. The values of concentration were computed using an integration time of five minutes corresponding to a height resolution of about 1500 km. This resolution is indicated by the vertical bars in the graphs. The uncertainties in the computed electron concentration are indicated by horizontal lines.

It is clear from Figure 2 that useful values of electron concentration could be obtained only in the height range from 6,000 to some 13,000 km and that the October data were substantially better than those obtained later on. Below 6,000 km the satellite elevation was too small to permit good measurements while above 13,000 the uncertainties became comparable to the quantity measured.

Figure 3 shows how the different uncertainties, on 17 October 1964, depended on satellite height. The total uncertainty, δn_S, was quite large at low altitudes, dropping to a constant value of about ± 600 electrons cm^{-3} at higher altitudes. The relative error becomes important at greater heights due to the diminishing electron concentration. The scaling error, δn_{S_1}, is inversely proportional to $\langle B_L \rangle$ (c.f. equation (20)) and tends to increase as the azimuth approaches 180°. Thus, for the early passes when the satellite rose eastward of the observing station and moved towards the south, the value of δn_{S_1} tended to grow during the run. The opposite occurred in the December pass. Note that the scaling error was, by far, the dominant error in the 17 October run. The "model" error, δn_{S_2}, is proportional to $d\Omega/dt$, (c.f. equation (24)) and, therefore, depends strongly on the rate of change of the zenithal angle. For this reason this error is always larger in the beginning of the run. The error, δn_{S_3}, due to temporal variations of the profile shape is quite small (compared with other errors) and can be neglected. Both the uncertainties due to horizontal gradients and due to the neglect of the three integrals in equation (17) depend on $d\varphi_o/dt$ and on $\sin \varphi_o \; (d\alpha/dt)$ i.e., depend on the rate of change of the zenithal angle and of the azimuth of the satellite. These errors were small in October but became dominant towards the end of the year. They do decrease as the satellite height increases and go through zero when the beacon is at 30,000 km, but at this altitude the local electron concentration is so small that the total errors from other sources are much bigger than the concentration itself.

Figure 4 shows the manner in which the total uncertainty (at a height of 7,000 km) varies from one pass to another. It can be seen that the most favorable conditions occurred near the middle of October. In Figure 5 the OGO-I beacon data are compared with two electron concentration profiles obtained with ion spectrometers. One profile is for 31 October 1964 and was derived from OGO-I spectrometer data [Brinton, Pickett and Taylor, 1968] and the other is from a similar instrument mounted on OGO-III and corresponds to an inbound (nighttime) pass of the satellite on 19 July 1966 [Taylor, Brinton and Pharo, 1968]. These profiles were scaled from the published graphs and for this reason are not precisely

accurate representations of the authors' values. It is seen that the values determined from the radio beacon observations bracket those of the comparison profiles. The differences may be due to diurnal and day-to-day variations since the spectrometer data and the beacon data were taken at different dates and different times of day.

In order to compare the beacon results with the equatorial electron concentrations derived from whistler data, the values of concentration from the OGO-I experiment were mapped onto the equatorial plane in the manner described below.

Assuming uniform temperature in the protonosphere, the electron concentration, n, at a point on a given geomagnetic field line is related to the concentration, n_o, at another point of the same line by the expression [Angerami and Thomas, 1964];

$$n = n_o \exp\left[\frac{R_o}{H_o}\left(\frac{R_o}{R} - 1\right)\right]$$

$$H_o = \frac{k\,(T_e + T_i)}{m\,g_o} \qquad (33)$$

where R is the geocentric distance

k is the Boltzmann constant

T_e and T_i are, respectively, the electron and ion temperatures.

m is the mass of the proton

g_o is the acceleration of gravity at the distance R_o.

Figure 6 shows the whistler results of Angerami and Carpenter [1966] and Smith and Angerami [1968] as well as the extrapolated OGO-I values. The OGO-I values were obtained by assuming a plasma temperature of 3,000 K believed to be representative of daytime condidtions in October 1964 [Evans, 1967]. If a lower temperature were used, the values would be somewhat lower, but the reduction would not be very great. The whistlers were recorded on 6 June 1963 at 01:50 local time at Eights in Antartica when extremely quiet geomagnetic conditions prevailed. The data were reduced under the assumption of hydrostatic equilibrium in the protonosphere and a plasma temperature of 1,200 K. This temperature appears somewhat low, but the results would not be significantly different if a

higher temperature had been used. Whistler and beacon results differ by a factor of two which has not yet been explained. One might be tempted to attribute the discrepancy to a large day-to-night variation. Such variations have not been previously reported and the nighttime data of Taylor et al. in Figure 5 seem to contradict this explanation.

Using equation (33), it is also possible to map the OGO-I results onto a horizontal surface at 1,000 km altitude and thus compare the beacon values with those from Alouette I. These latter data are reported by Thomas, Rycroft, Colin and Chan [1965] for the 1,000 km level in the winter of 1963. The OGO-I data for 17 October 1964 were extrapolated to the same height using pure hydrogen plasma at 3,000 K. Since it is probably that a substantial quantity of oxygen ions exists at these altitudes, it can be expected that smaller scale heights than those used in the computation prevailed in the neighborehood of the level of interest. If this fact had been taken into account, the OGO-I values would be higher than indicated in Figure 7, where the comparison is made. This effect would be more noticeable the higher the geomagnetic latitude (where there is more O^+) and would contribute to the straightening out of the graph bringing it into closer parallelism with the Alouette curve.

VI - CONCLUSIONS

The theoretical discussion in section IV has shown that propagation experiments of the type discussed in this paper can be used as a means for determining protonospheric electron concentrations, provided adequate orbits are selected for the beacon satellite. The prime requirement of such orbits are low perigee and high eccentricity so that large vertical velocities and low altitudes are combined. The high eccentricity, however, makes the satellite sensitive to the perturbing influence of other celestial bodies, in particular to the moon For this reason, OGO-I had a perigee which increased very fast from its initial value of some 280 km, and its orbit became progressively less favorable for the present experiment restricting the usefulness of the satellite to the first few months after launch when electron concentrations could be determined between some 6,000 and 15,000 km.

The main limitations of the experiment are the large uncertainties in the measured values of local electron concentration. These uncertainties stem in great part from difficulties in scaling $d\Omega/dt$ and are dependent on the integration time used. The height resolution is an inverse function of this integration time so that the product (height resolution x uncertainty in concentration) is of the order 5×10^5 km x cm^{-3}; a five minute integration time results in scaling errors of about ± 300 el.cm^{-3} and a height resolution of 1,500 km.

A major improvement in the scaling error would result from the use of a non-spinning, earth oriented satellite. The Faraday angle changes could then be measured accurately by a spinning ground antenna.

Other important sources of uncertainty are the possible presence of unknown horizontal gradients of concentration and the necessity to estimate (from assumed models) the magnitude of a number of terms in the expression giving the local electron concentration.

After estimating all of these uncertainties, electron concentration profiles have been obtained on four days, as shown on figure 2. Although the analysis has been considerably more involved than would be desired, the electron concentrations obtained are valid in an altitude region

difficult to measure by whistlers or incoherent scatter sounders and in which direct measurements with probes are difficult to interpret.

BIBLIOGRAPHY

Angerami, J.J. and D.L. Carpenter, Whistler studies of the plasmapause in the magnetosphere. 2. Equatorial density and total tube electron content near the knee in magnetospheric ionization, J. Geophys. Res., 71, 711, 1966.

Angerami, J.J. and J.O. Thomas, The distribution of electrons and ions in the earth's exosphere, J. Geophys. Res., 69, 4537, 1964.

Brinton, H.C., R.A. Pickett and H.A. Raylor, Jr., Thermal ion structure of the plasmasphere, Planet. Space Sci., 16, 899, 1968.

da Rosa, A.V., Eccentric geophysical-observatory satellite S 49. Interpretation of the radio-beacon experiment, Technical Report No. 1, NASA contract NASr-136, Stanford University, Radioscience Lab, 1965a.

de Mendonça, F., Ionospheric electron content and variations measured by Doppler shifts in satellite transmissions, J. Geophys. Res., 67, 2315, 1962.

Evans, J.V., Millstone Hill Thomson scatter results for 1964, Tech. Rep. 430, Lincoln Lab. M.I.T., 1967.

Ross, W.J., Second-order effects in high-frequency transionospheric propagation, J. Geophys. Res., 70, 597, 1965.

Ross, W.J., The determination of electron content from satellite Doppler measurements, J. Geophys. Res., 65, 2601, 1960.

Ross, W.J., O.K. Garriott, F. de Mendonça, and A.V. da Rosa, Comments on local electron density determination from Doppler dispersion measurements of satellite radio beacons, J. Geophys. Res., 73, 1102, 1968.

Seddon, J.C., A.D. Pickar and J.E. Jackson, Continuous electron density measurements up to 200 km, J. Geophys. Res., 59, 513, 1954.

Smith, R.L. and J.J. Angerami, Magnetospheric properties deduced from OGO-I observations of ducted and non-ducted whistlers, J.Geophys.Res., 73, 1, 1968.

Taylor, Jr., H.A., H.C. Brinton and M.W. Pharo, III, Contraction of the plasmasphere during geomagentically disturbed periods, J. Geophys. Res., 73, 961, 1968.

Thomas, J.O., M.J. Rycroft, L. Colin and K.L. Chan, Electron density profiles in ionosphere and exosphere, Proc. NATO Adv. Study Inst., Norway, Apr. 1965.

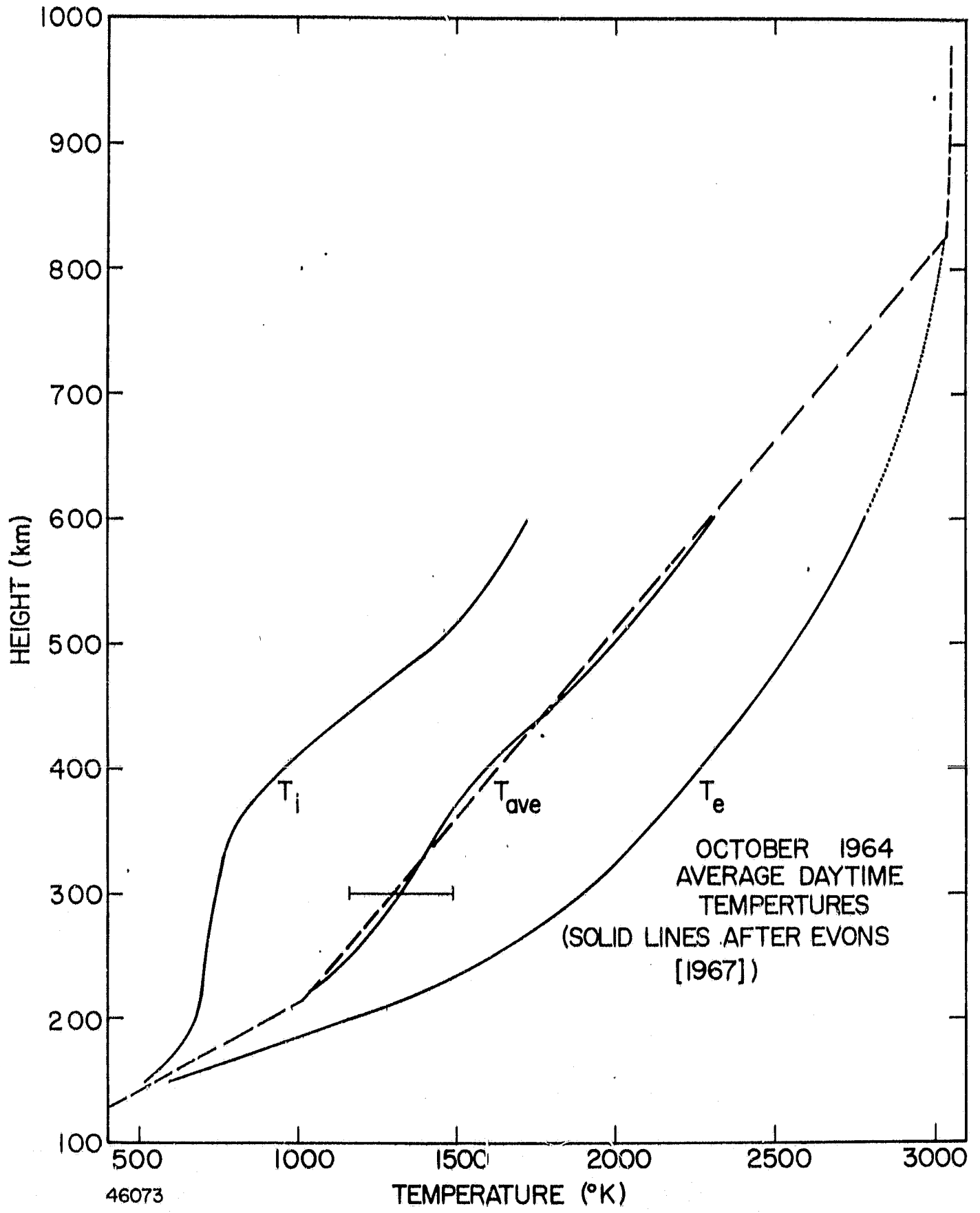
1000
900
800
700
600
500
400
300
200
100
HEIGHT (km)
500
1000
1500
2000
2500
3000
TEMPERATURE (°K)
T_i
T_{ave}
T_e
OCTOBER 1964
AVERAGE DAYTIME
TEMPERTURES
(SOLID LINES AFTER EVONS
[1967])
46073

Figure 1

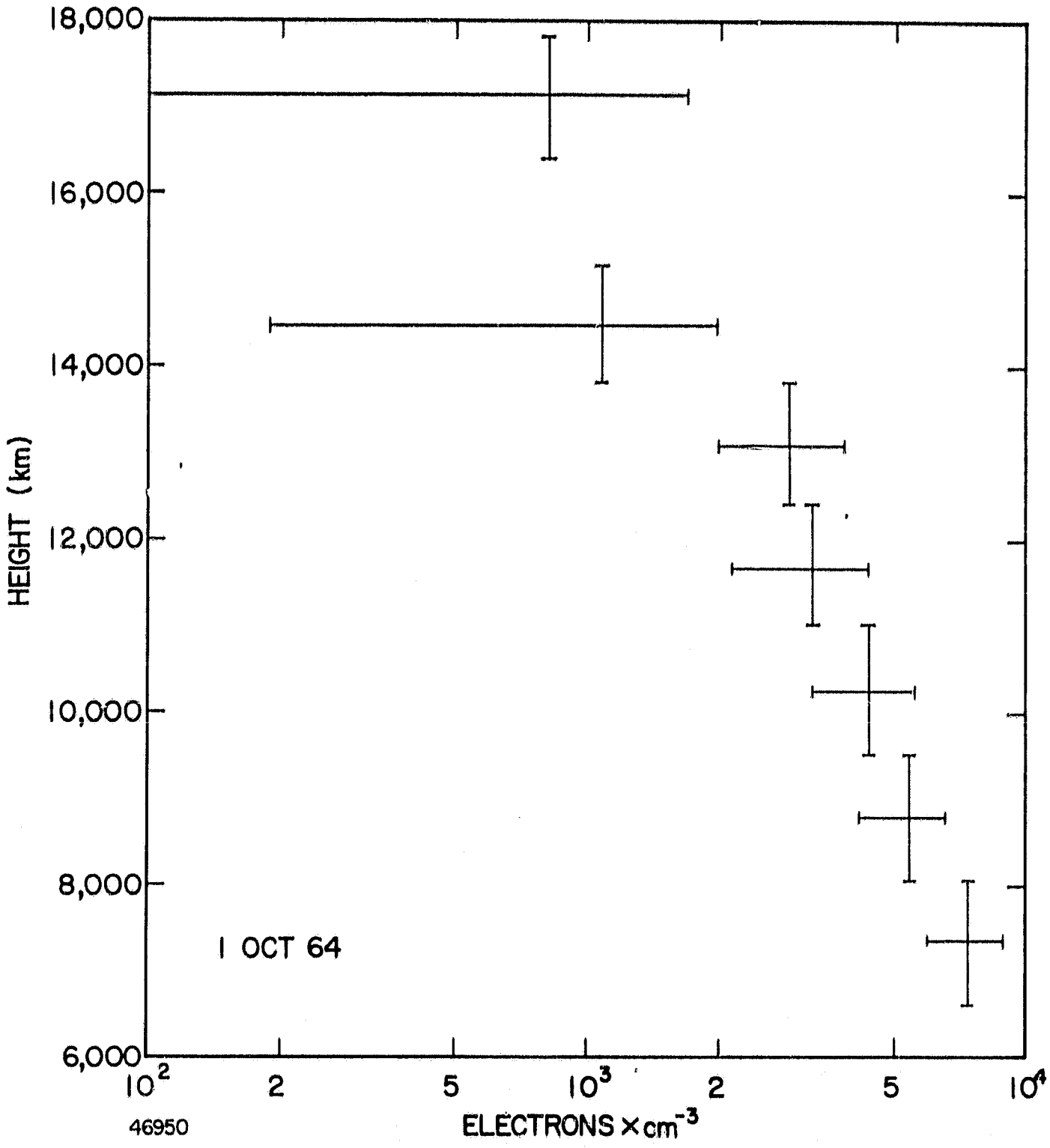
18,000
16,000
14,000
12,000
10,000
8,000
6,000
HEIGHT (km)
1 OCT 64
10^2
2
5
10^3
2
5
10^4
ELECTRONS × cm^{-3}
46950

Figure 2 A

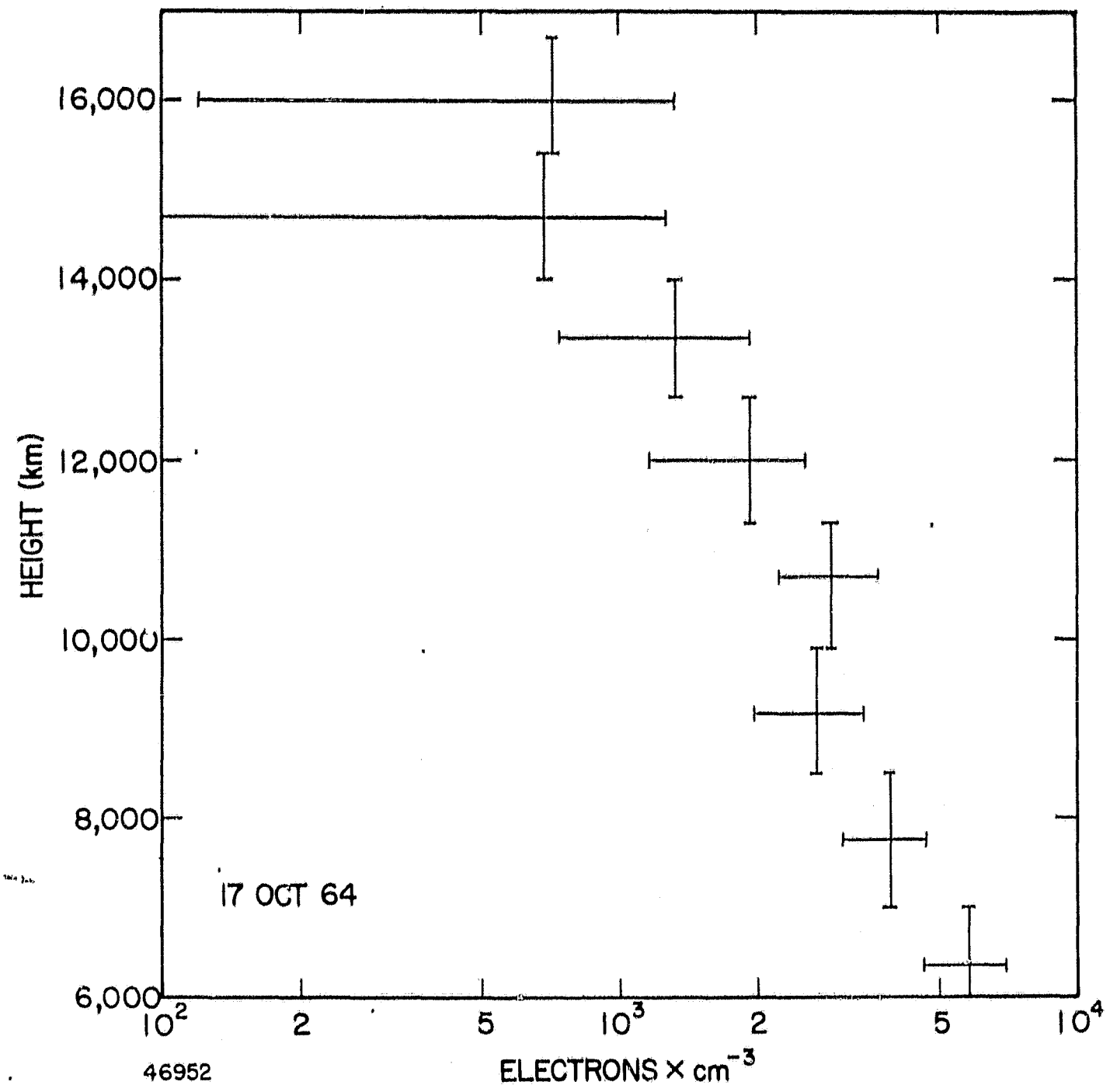
16,000
14,000
12,000
10,000
8,000
6,000
HEIGHT (km)
17 OCT 64
10^2
2
5
10^3
2
5
10^4
ELECTRONS × cm^{-3}
46952

Figure 2B

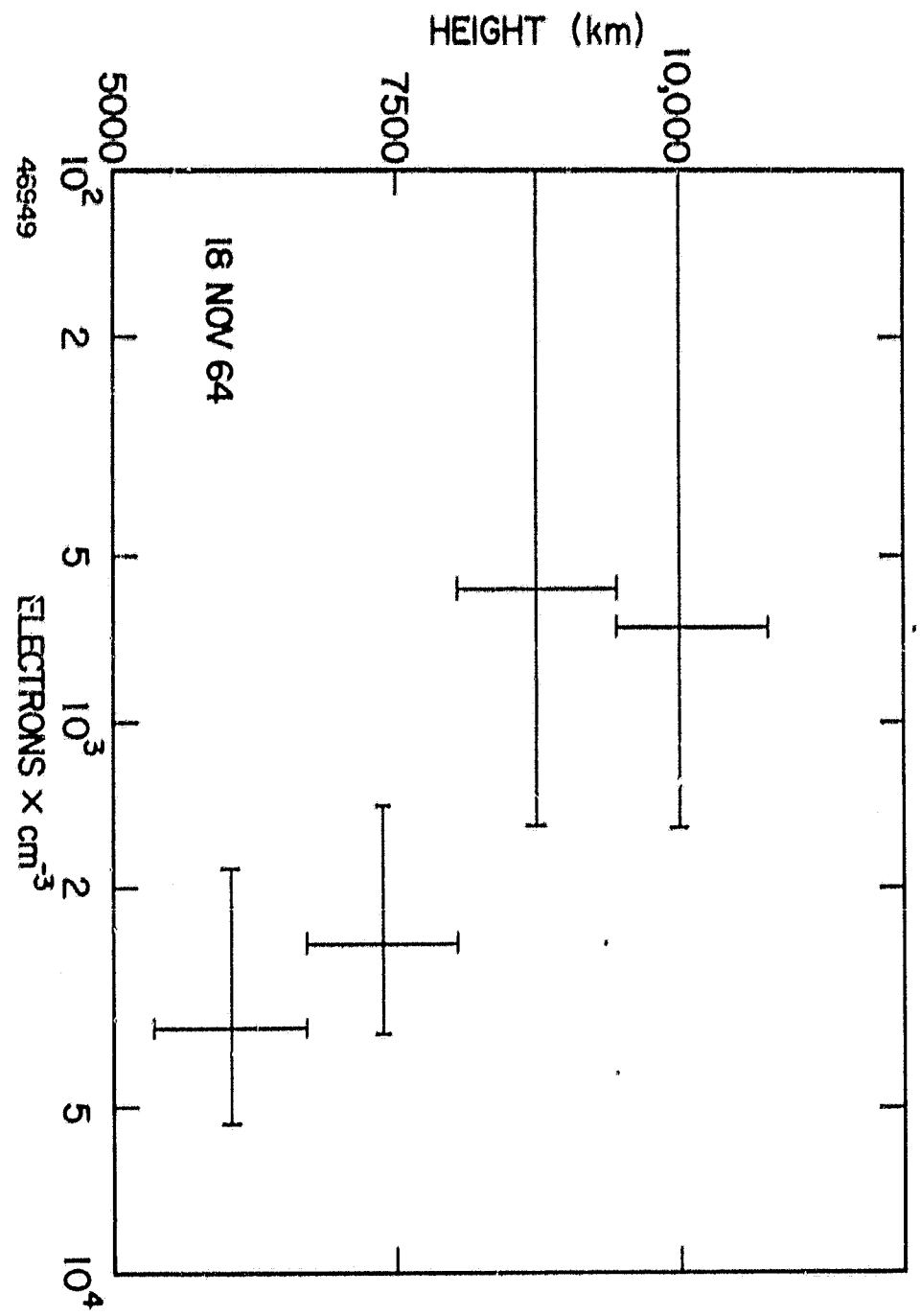
HEIGHT (km)
5000
7500
10,000
10^2
2
5
10^3
2
5
10^4
ELECTRONS X cm^{-3}
18 NOV 64
46549

Figure 2C

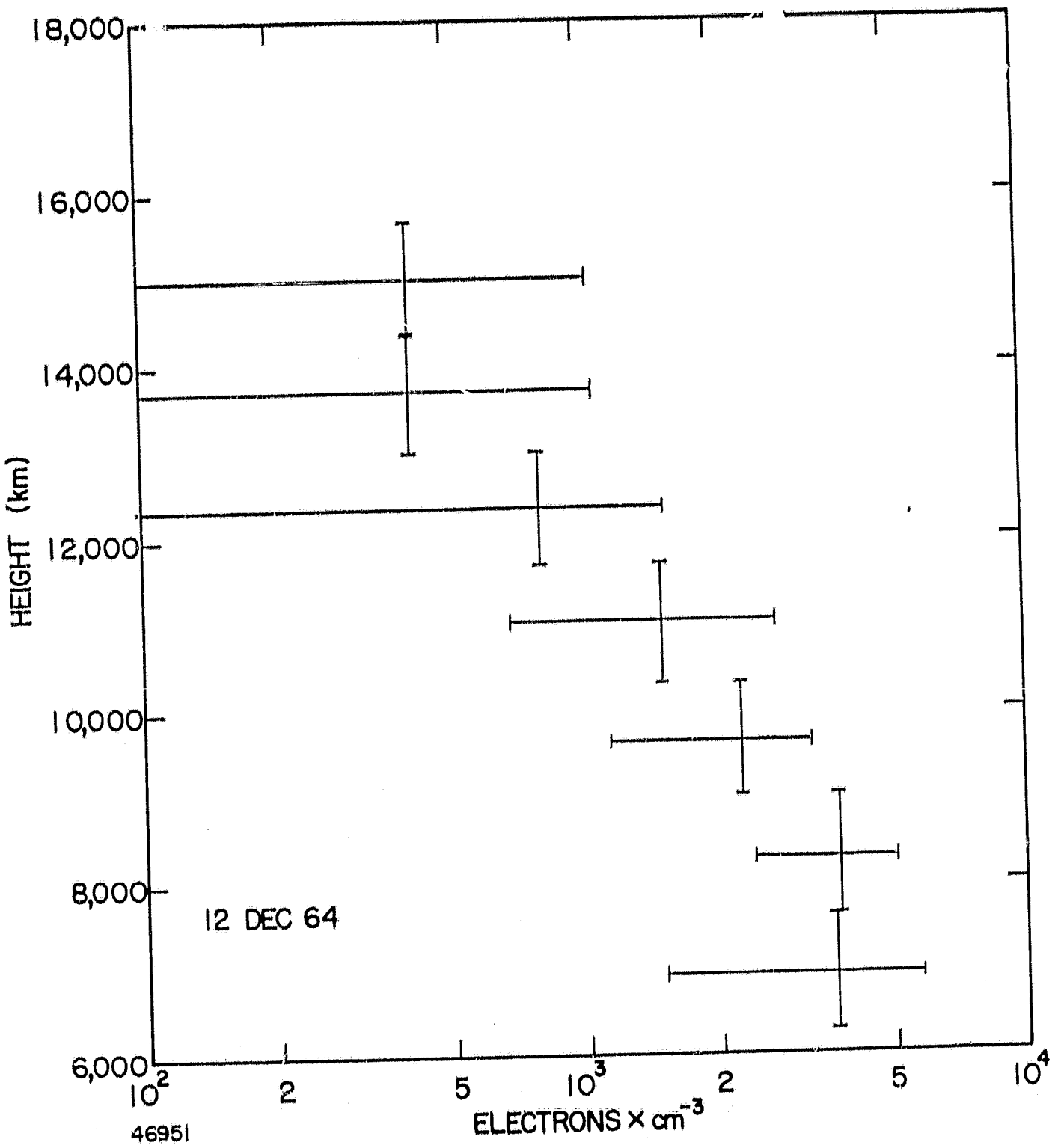
18,000
16,000
14,000
12,000
10,000
8,000
6,000
HEIGHT (km)
12 DEC 64
10^2
2
5
10^3
2
5
10^4
ELECTRONS × cm^{-3}
46951

Figure 2D

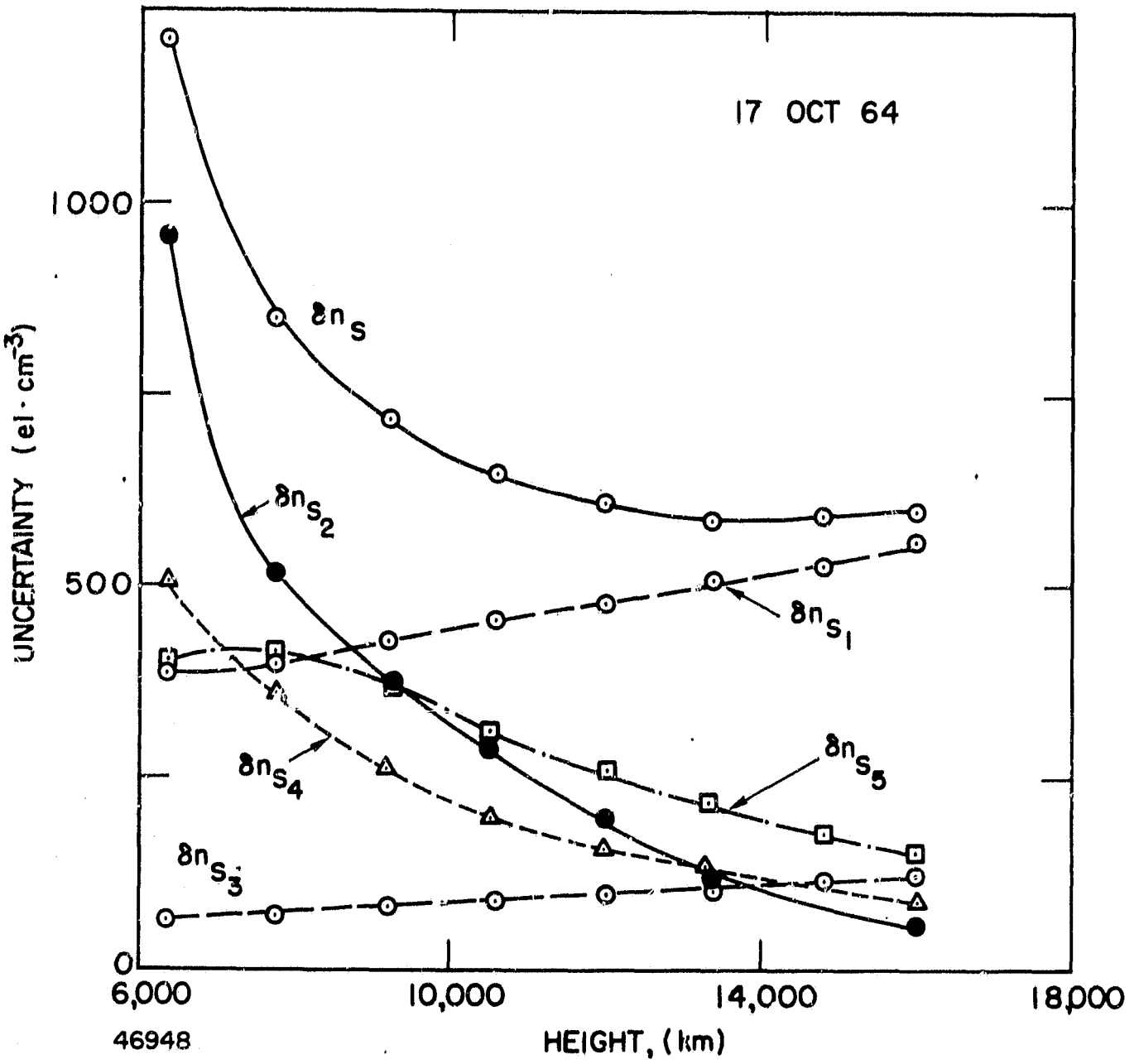
17 OCT 64
1000
500
0
UNCERTAINTY (el·cm⁻³)
δn_S
δn_S2
δn_S1
δn_S4
δn_S5
δn_S3
6,000
10,000
14,000
18,000
HEIGHT, (km)
46948

Figure 3

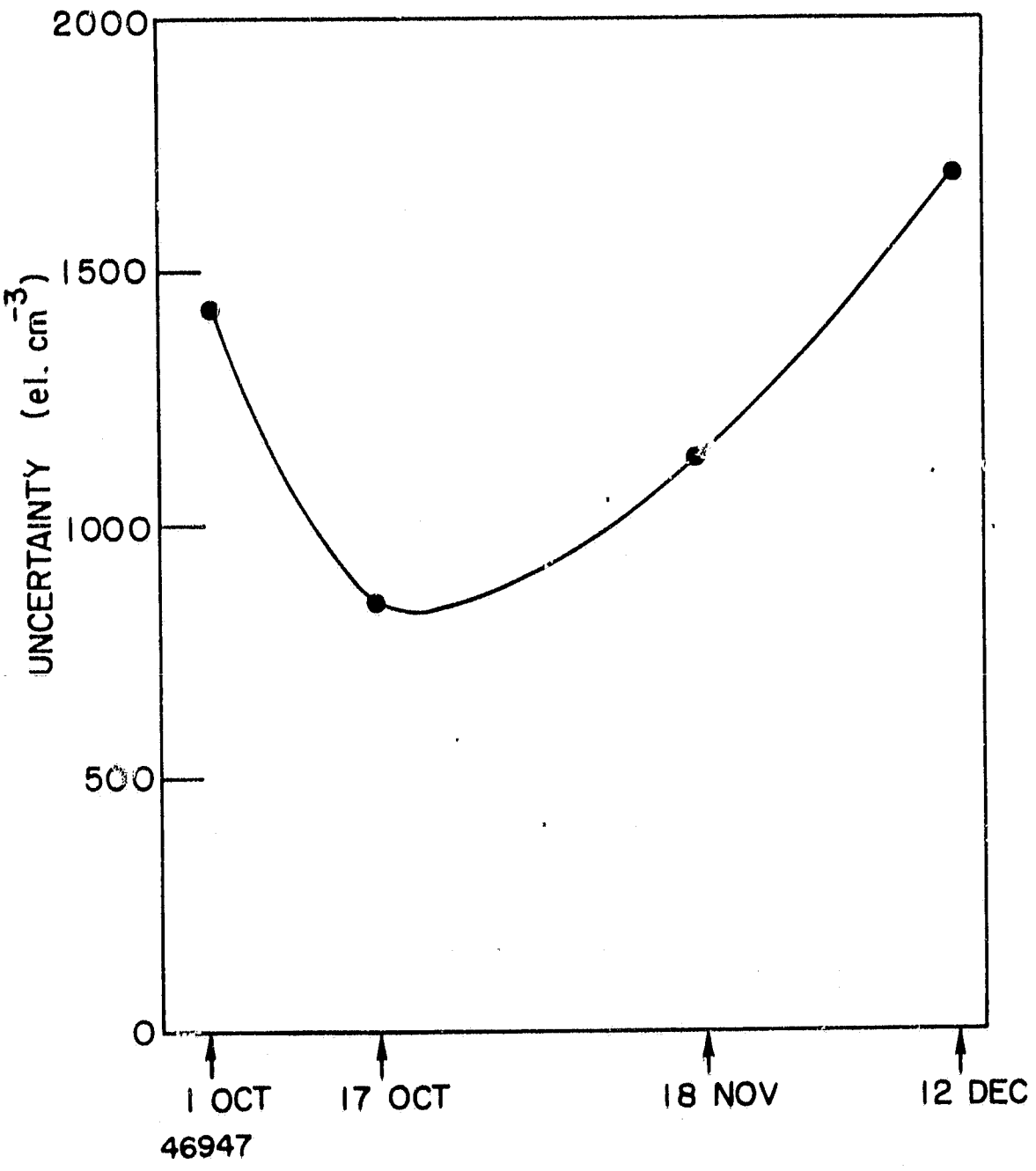
2000
1500
1000
500
0
UNCERTAINTY (el. cm^{-3})
1 OCT
17 OCT
18 NOV
12 DEC
46947

Figure 4

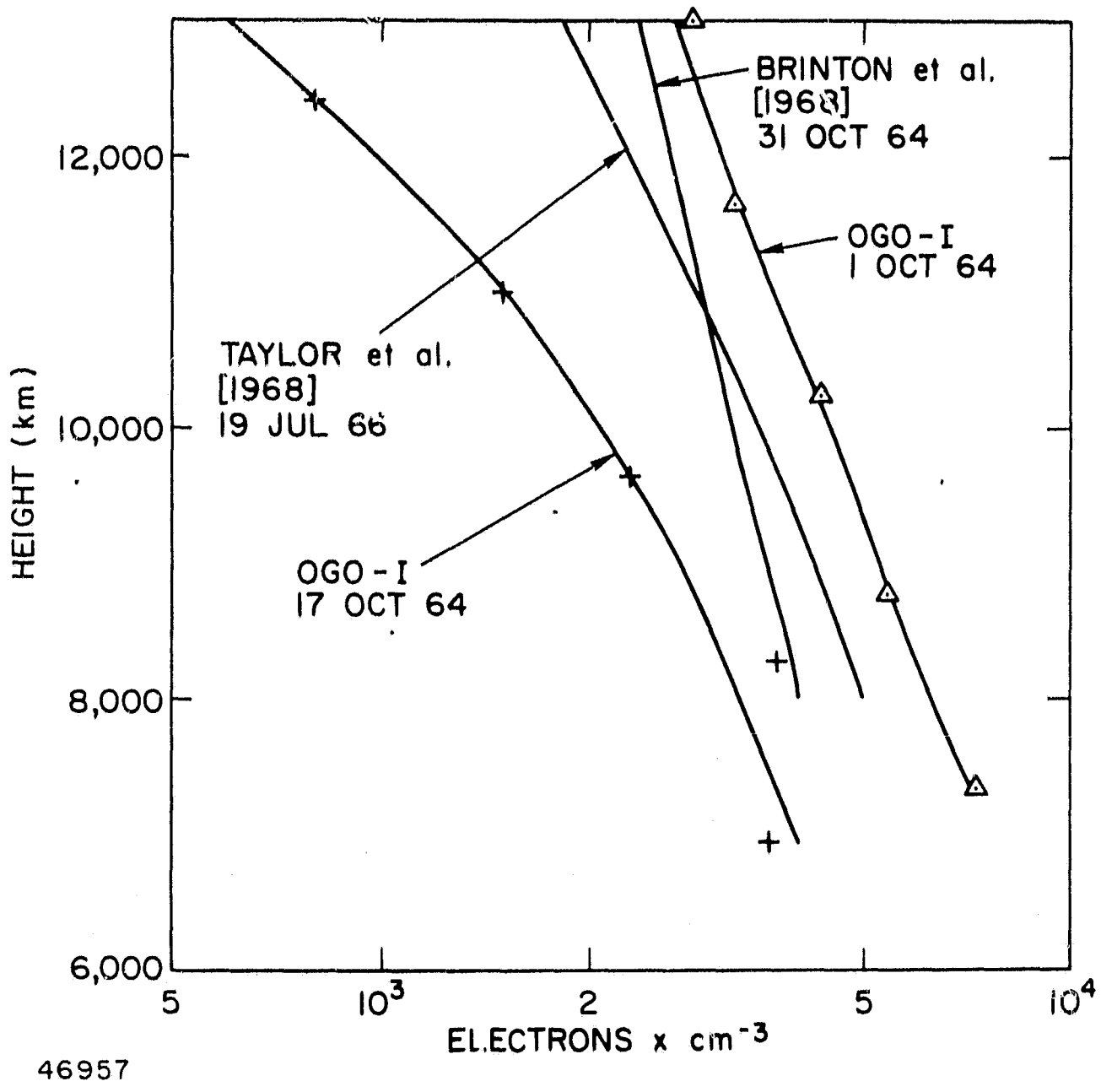
BRINTON et al.
[1968]
31 OCT 64
OGO-I
1 OCT 64
TAYLOR et al.
[1968]
19 JUL 66
OGO-I
17 OCT 64
12,000
10,000
8,000
6,000
HEIGHT (km)
5
10^3
2
5
10^4
ELECTRONS x cm^-3
46957

Figure 5

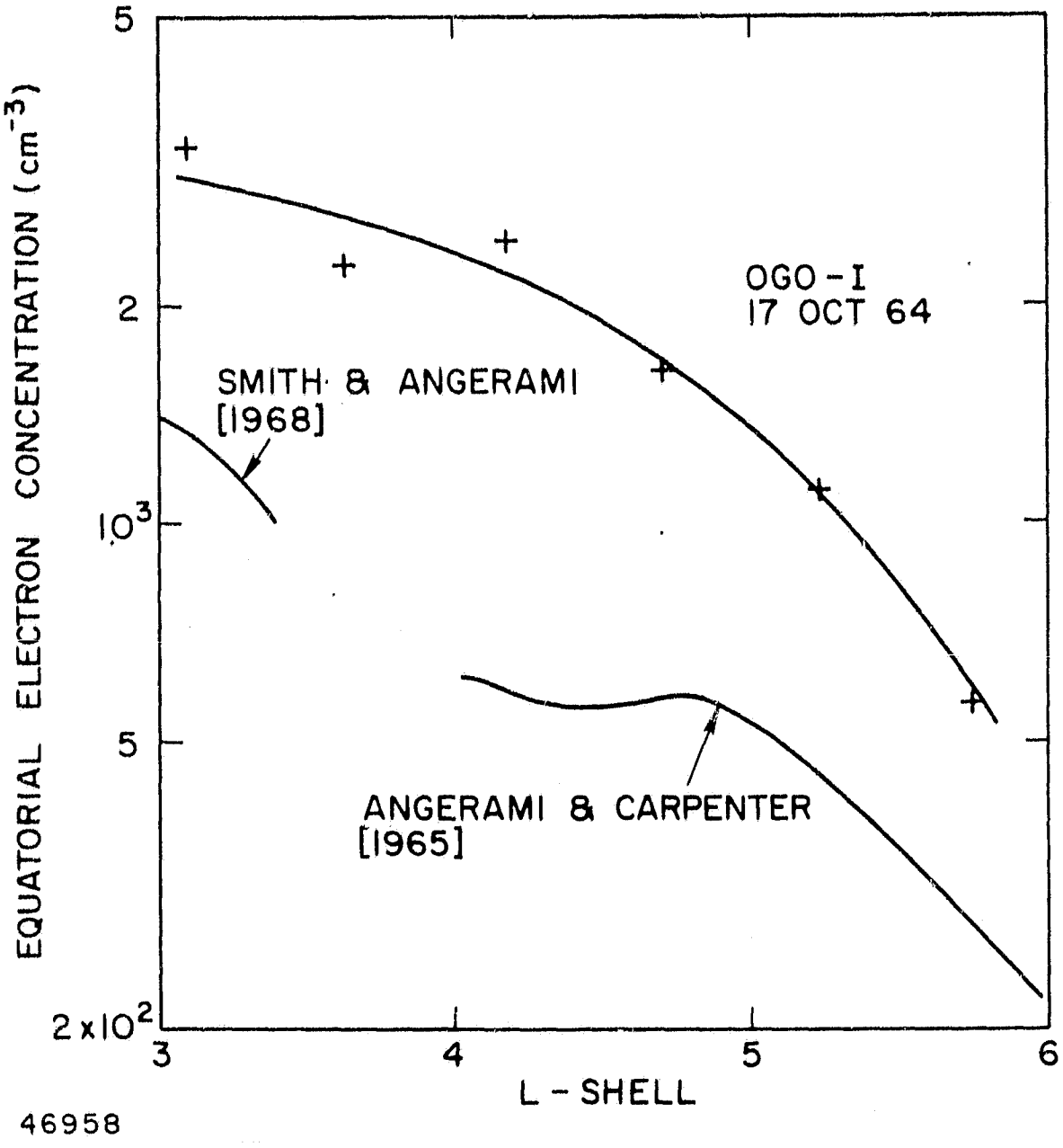
EQUATORIAL ELECTRON CONCENTRATION (cm^{-3})
5
2
10^3
5
2×10^2
3
4
5
6
L - SHELL
OGO - I
17 OCT 64
SMITH & ANGERAMI
[1968]
ANGERAMI & CARPENTER
[1965]
46958

Figure 6

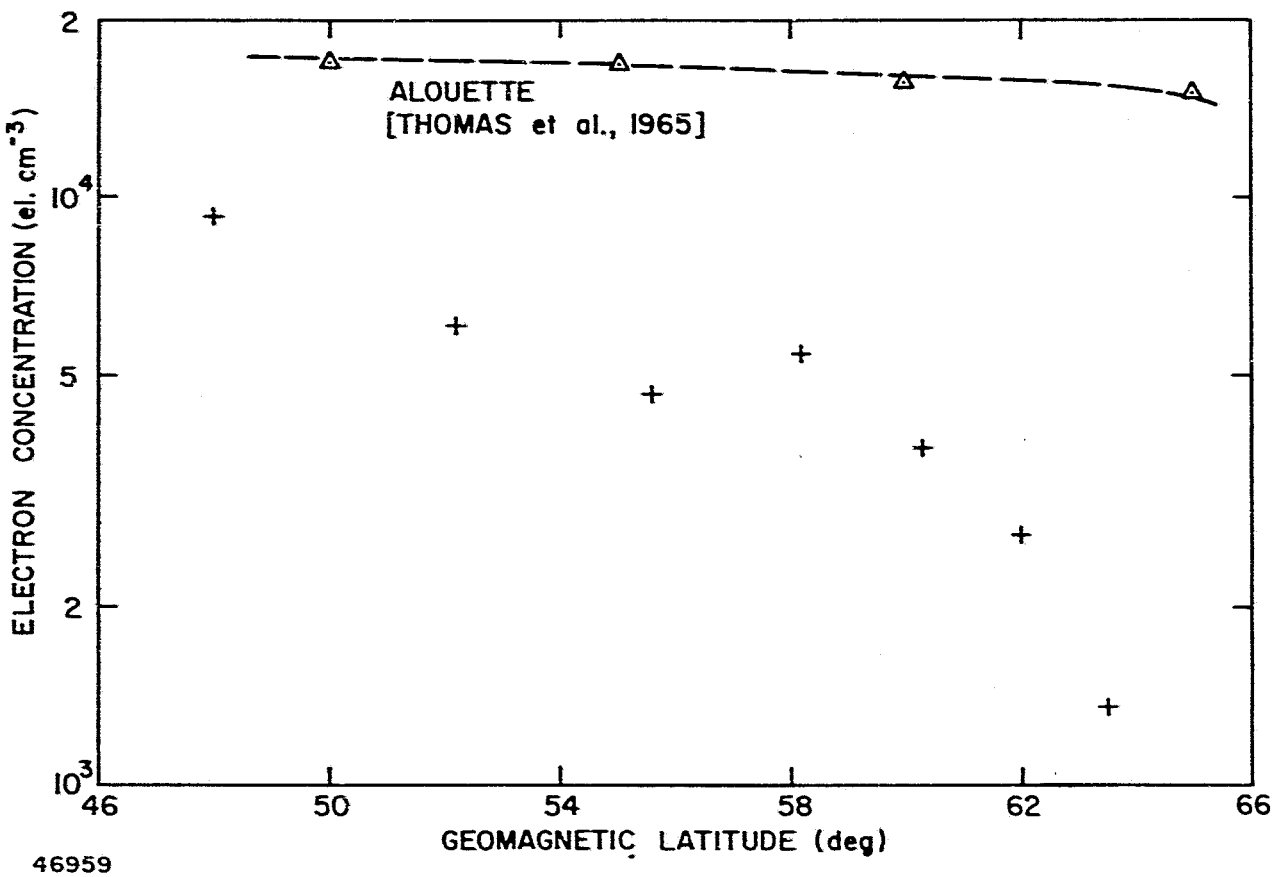
ALOUETTE
[THOMAS et al., 1965]
ELECTRON CONCENTRATION (el. cm⁻³)
2
10⁴
5
2
10³
46
50
54
58
62
66
GEOMAGNETIC LATITUDE (deg)
46959

Figure 7